Journal of Materials Chemistry A

Structure and Chemical Stability in Perovskite-Polymer Hybrid Photovoltaic Materials

Journal:	*Journal of Materials Chemistry A*
Manuscript ID	TA-ART-08-2018-007545.R1
Article Type:	Paper
Date Submitted by the Author:	29-Oct-2018
Complete List of Authors:	Fairfield, Daniel; Northwestern University Sai, Hiroaki; Northwestern University, Center for Bioinspired Energy Science Narayanan, Ashwin; Northwestern University Passarelli, James; Northwestern University Chen, Michelle; Northwestern University Palasz, Joseph; Northwestern University Palmer, Liam; Simpson Querrey Institute for BioNanotechnology , ; Northwestern University, Wasielewski, Michael; Northwestern University, Department of Chemistry Stupp, Samuel; Northwestern University,

Structure and Chemical Stability in Perovskite-Polymer Hybrid Photovoltaic Materials

Daniel J. Fairfield,[1] Hiroaki Sai,[1] Ashwin Narayanan,[1] James V. Passarelli,[2] Michelle Chen, [2] Joseph Palasz,[2] Liam C. Palmer,[2,4] Michael R. Wasielewski,[2] and Samuel I. Stupp[,1,2,3,4,5]*

[1]Department of Materials Science and Engineering, Northwestern University, Evanston, Illinois 60208, USA, [2]Department of Chemistry, Northwestern University, Evanston, Illinois 60208, USA, [3]Department of Medicine, Northwestern University, Chicago, Illinois 60611, USA, [4]Simpson Querrey Institute, Northwestern University, Chicago, Illinois 60611, [5]Department of Biomedical Engineering, Northwestern University, Evanston, IL 60208, USA.

*s-stupp@northwestern.edu

Abstract:

Adding polymers to methylammonium lead iodide perovskite solar cell active layers has been previously shown to increase their chemical stability, but stabilization mechanisms in these hybrid materials are poorly understood. We report here on a structural and spectroscopic analysis in a number of perovskite-polymer hybrid materials and compare their stability. We observed that perovskite crystallite sizes decrease with the addition of polymers (polyethylene glycol, polyethyleneimine, poly(acrylic acid) and polyvinylpyrrolidone), and through the use of nanomechanical AFM showed phase contrast in the perovskite-polymer mixture. NMR and single-crystal growth experiments reveal that acid-base interactions, as well as facet-dependent interfacial interactions between perovskite and polymer, contribute to differences in stabilities of these hybrid materials. The polymers investigated tend to suppress the formation of a hydrate crystal phase that accelerates the degradation reaction, and we report that adding poly(acrylic acid) increases significantly the stability of perovskite films under humid air and ambient illumination. Under these controlled degradation conditions, perovskite-poly(acrylic acid) hybrid solar cells maintain stable efficiency for the first 3 days and then slowly degrade over the next 6 days under humid air and illumination, whereas control perovskite solar cells degrade entirely within the first 2 days. These results highlight the importance of choosing suitable functional groups in the polymer phase of perovskite hybrid solar cells to prolong their device lifetime.

Introduction

Methylammonium lead iodide ($MAPbI_3$) forms perovskite crystals via solution processing with promising optoelectronic properties for photovoltaics including high carrier mobility,[1,2] high absorption coefficient in the visible and near-infrared spectrum,[3] and balanced ambipolar transport.[4,5] Perovskite solar cells (PSCs) have shown impressive gains in power conversion efficiency over the past 6 years, from their first demonstration as sensitizers in 3.8% efficient dye sensitized solar cells[6] to a champion efficiency of >22% [7] through the use of cation (formamidinium and cesium) and anion (chloride, bromide) alloys in the active layer in addition to many incremental device engineering improvements. Developments such as mesoporous scaffolds,[8] two-step active layer processing,[9] planar heterojunctions,[10] organic charge transport layers,[11] and compositional tuning[12] have all played a role in the improvements of these devices. However, the chemical instability of perovskite active layers has been a significant hindrance to the widespread commercialization of this technology.

$MAPbI_3$ solar cells are known to degrade in the presence of humidity, light, or oxygen, and many different decomposition mechanisms have been proposed and studied.[13,14,15,16,17] One proposed decomposition mechanism is the formation of hydroiodic acid and gaseous methylamine through an acid-base reaction when water is added to methylammonium iodide (MAI).[14] The first step in this degradation pathway can be the formation of a solvate phase with atmospheric humidity.[14] *N*,*N*-dimethylformamide (DMF), dimethyl sulfoxide (DMSO), and water can all form solvates with the perovskite, a fact that has been used to beneficially control crystal growth and formation of thin films.[15,16] The solvate that $MAPbI_3$ forms with water, $(MA^+)_2(PbI_3^-)\cdot(H_2O)_2$, is an important species in the degradation process of the active layer since it forms reversibly and spontaneously at room temperature in a high humidity environment.[16] A

recent study has also shown that even under dry conditions, the combination of oxygen and light also degrades the perovskite rapidly.[17] The proposed mechanism for this degradation pathway is the formation of superoxide O_2^- when O_2 reacts with photo-generated electrons in the perovskite layer.[17] O_2^- then degrades the perovskite structure to methylamine, PbI_2, water, and I_2. Because of these proposed degradation mechanisms, and likely many others that have yet to be identified, non-encapsulated PSC devices are only stable for hours, and even encapsulated devices are only stable on the timescale of days in conditions relevant to stable outdoor operation.[18,19]

Recent studies have shown that either small molecules[20,21,22] or polymers[23,24,25,26,27,28,29] can be added to the active layer to improve the active layer morphology and stability of PSCs. In the case of organic surface modifiers,[20] in one study only ~3 mol% of the MAI was replaced with alkylammonium phosphonate in the precursor solution. They propose that this zwitterionic molecule bonds to grain boundaries of the $MAPbI_3$ crystals, and that hydrogen bonding interactions between the phosphonic acid and MAI are important in stabilizing the $MAPbI_3$. Indeed, other ammonium iodide species, such as phenylethylammonium iodide, have been shown to contribute to stability of the $MAPbI_3$ perovskite even at very low concentrations by forming quasi-two-dimensional (2D) layers within $MAPbI_3$ crystals[30]. These bulky cations replace methylammonium in the lattice and enhance stability by forming more robust capping layers at grain boundaries.[30] With higher amounts of cation substitution, perovskite crystals can form Ruddlesden-Popper or pure n=1 2D phases with better stability at the cost of some optoelectronic performance.[31,32,33,34] Thus, these reports support the idea that molecular species with ammonium functionality can substitute into the crystal lattice to stabilize the overall structure while maintaining a single phase. Polymers have been known to increase the stability of $MAPbI_3$ active layers without substitution into the crystal lattice.[23,24,25,26] Adding polymers to the

spin-coating solution increases the viscosity of the solution, which in turn increases the thickness, slows the drying rates, and changes the crystallization pathways of the perovskite active layer.[27,29] This could be considered analogous to some small molecule additives to organic and perovskite photovoltaics, where additives such as 1,8-diiodooctane and chloronaphthalene are added to the spin-coating solution to control crystallization of the active layer.[35,21,22] However, in contrast to these small molecule additives, polymers remain in the active layer after annealing to form a two-phase hybrid film. When 3–6 wt% of polymer is added to the perovskite precursor solution, it can comprise up to 25 vol% of the active layer when accounting for density differences between the perovskite (4.1 g/cm^3)[36] and typical polymer phases (~1.2 g/cm^3). Because of the significant volume fraction of polymer present in these films, phase separation between the perovskite and polymer occurs, and examining the morphology of these perovskite-polymer hybrid films as two-phase systems is critical to understanding their properties. Previous studies[23,24,25,26] have investigated the use of uncharged polymers such as polyethylene glycol (PEG), poly(methyl methacrylate), polydimethylsiloxane-urea, and polyvinylpyrrolidone (PVP) to improve the stability of PSCs. Each of these studies demonstrated improved device stability with added polymer compared to control $MAPbI_3$ devices under controlled humidity conditions without illumination. The extent of added stability claimed in these studies has yet to be systematically analyzed because the exact device and degradation conditions do vary. [37]

Polyvinylpyrrolidone (PVP), poly(acrylic acid) (PAA), and polyethyleneimine (PEI) were investigated recently as grain boundary modifiers in PSCs.[38] These polymers were added to the perovskite precursor solution in a 1:1000 polymer:MAI ratio which is significantly less polymer than that used in previous studies on polymer hybrids. They proposed that PVP interacts with $MAPbI_3$ to passivate the grain boundaries, which increases efficiency and enhances stability

in encapsulated devices stored inside of a glovebox. While their study highlighted the utility of polymers in improving device efficiency through grain boundary engineering, the link between polymer functionality and degradation pathways in operating conditions remains unexplored.

In this work we investigate the microstructural changes induced by the introduction of four polymers, PEG, polyethyleneimine (PEI), PVP, and PAA in the active layer and the mechanism by which the stability is improved by these polymers. We then investigate the effect of polymer inclusion on the stability and performance of PSCs under humid air and ambient light. Understanding how polymers interact with perovskite phases and how the perovskite-polymer hybrid films form is critical to gain an understanding of how macromolecules improve the stability of PSCs. This mechanistic understanding is also important in finding possible strategies to minimize the negative impact polymeric phases have on their optoelectronic properties.

Experimental Section

Chemicals Lead iodide (PbI_2-99% perovskite grade) was purchased from Tokyo Chemical Inc. Poly(3,4-ethylenedioxythiophene) polystyrene sulfonate (PEDOT:PSS) was purchased from Heraeus. All other chemicals were used as received from Sigma-Aldrich.

Methylammonium iodide synthesis As described in the literature,[39] methylamine solution (40% in methanol) was reacted with hydroiodic acid (57% in water) in a round bottom flask stirring in an ice bath. The solvent was removed with rotary evaporation at 60°C, and then the MAI was dissolved in ethanol. MAI was precipitated from solution with diethyl ether. The MAI powder was then dried in a vacuum oven at 60°C overnight.

Characterization Tapping mode atomic force microscopy (AFM) measurements were carried out using a Bruker ICON system. Nanomechanical AFM measurements were utilized a Veeco Bioscope Catalyst AFM with a ScanAsyst-Air silicon nitride AFM probe with a stiffness of 0.4 N/m, and a nominal tip radius of 5 nm. 0.3–1.2 nN of force was applied to the sample to measure mechanical behavior, and our data was analyzed with Bruker Nanoscope Analysis software. Force-loading curves were modeled using the Derjaguin, Muller and Toporov (DMT) model[40] to calculate the local elastic modulus. Profilometry measurements to determine film thickness were performed on a Veeco Dektak 150 surface profiler. X-ray diffraction (XRD) experiments were conducted on a Scintag XDS2000 using Cu Kα radiation at 40 kV and 20 mA of current, and scanning electron microscopy (SEM) was performed using a Hitachi SU8030. Transmission electron microscopy (TEM) experiments were performed using a Hitachi HT-7700 at 120 kV accelerating voltage (the thickness of samples cast on TEM grids had to be thinner than typical PSC film thicknesses (~150 nm) in order to see contrast). We prepared TEM samples by drop casting 10 μL of solution onto a lacey carbon grid and wicking away the excess solution.

Samples were then annealed for 10 minutes at 120°C and 10 minutes at 100°C. ^{1}H nuclear magnetic resonance (NMR) spectroscopy was performed using an Agilent DD2 500 MHz instrument. For sample preparation, dimethylsulfoxide-d_6 was dried with 4 Å molecular sieves overnight, and the polymer, MAI, and PbI_2 were dissolved in a total solid concentration of 200 mg/mL. The mass ratio of the perovskite precursors to polymer was kept at 15:1. Fourier transform infrared (FT-IR) spectroscopy was carried out using a Thermo Nicolet Nexus 870 spectrometer in transmission mode with perovskite films ground into a KBr pellet.

Steady-state photoluminescence (PL) spectra were collected on a Horiba Nanolog fluorimeter with an excitation wavelength of 525 nm. The PL spectra were collected using front-face detection and corrected for CCD-detector spectral response functions and monochromator wavelength dependence. Time-resolved photoluminescence (TR-PL) data were collected using a Hamamatsu C4334 Streakscope streak camera system with a 525 nm excitation wavelength. Data were collected with 5 to 500 ns windows with an instrument response function of ~2% of the experimental window. Excitation pulses were generated with a commercial direct-diode-pumped 100 kHz Amplifier (Spirit 1040, Spectra-Physics) that produced a fundamental beam of 1040 nm. The 1040 nm fundamental beam pumped a non-collinear optical parametric amplifier (Spirit-NOPA, Spectra-Physics), which delivered tunable, high-repetition-rate pulses at 525 nm (0.15 nJ/pulse).

Substrate preparation Patterned ITO substrates (Thin Film Devices, 20 ohms/square) were cleaned by sequential sonication in hexane, soapy water, milli-q water, and a 1:1:1 mixture of ispropanol, acetone, and methanol. After drying, clean substrates were treated for 20 minutes in a UV-ozone cleaner (Bioforce Nanosciences). Poly(3,4-ethylenedioxythiophene) polystyrene sulfonate (PEDOT:PSS) was filtered through a 0.45 μm nylon filter before spin-coating at 5000

RPM with a 1000 RPM/second ramp rate for 60 seconds. PEDOT:PSS films were then annealed at 150°C for 20 minutes in the glovebox.

Single Crystal growth Single crystals were grown via vapor diffusion from 20 wt% solutions of $MAPbI_3$ in γ-butyrolactone (GBL) using dichloromethane as the volatile nonsolvent for crystallization. Polymers were added to the crystallization solution before crystallization at a concentration of 20 mg/mL in GBL.

Device fabrication Devices were fabricated in a nitrogen-filled glovebox. The spin coating procedure for the active layer follows a slightly modified procedure from that outlined by Jeon et al.[15] For control devices, $MAPbI_3$ solutions were dissolved in a solvent mixture of 70% γ-butyrolactone (GBL) 30% dimethyl sulfoxide (DMSO) overnight under stirring and heating at 65°C. The active layer was spin-cast onto PEDOT:PSS-coated ITO substrates for 10 seconds at 1000 RPM and 15 seconds at 5000 RPM, and then 700 μL of toluene was cast on the spinning substrate and spun for 5 seconds at 5000RPM. For experimental devices, $MAPbI_3$ solutions with polymer additives were dissolved in mixtures of 80% dimethylformamide (DMF) and 20% DMSO.[41] The active layer was then spin-cast for 10 seconds at 1000 RPM and 20 seconds at 4000 RPM , and then 150 μL of chlorobenzene was drop cast on the spinning substrate and spun for 40 seconds at 4000RPM. The spin-cast layers were annealed at 120°C for 10 minutes followed by 10 minutes at 100°C. The over-layer solution was a 16 mg/mL solution of PCBM spin-cast at 2000 RPM. This solution was dissolved with stirring and heating at 65°C overnight before spin-coating the solution (filtered through a 0.2 μm PTFE filter). Bathocuproine (BCP) was dissolved at 0.5 mg/mL in ethanol and spin cast onto a 5000 RPM substrate. 50 nm gold contacts were thermally evaporated onto the substrates at a pressure of $<10^{-6}$ mbar using a

shadow mask to define 4 mm^2 devices. Finally, devices were tested in air on a Newport solar simulator with a Keithley 2400 sourcemeter.

Long term stability testing Polymers and perovskite-polymer blends were tested for long term stability using saturated salt solutions inside sealed bell jars. Lithium chloride (11% relative humidity (RH)), potassium acetate (23% RH), potassium carbonate (43% RH), calcium nitrate (55% RH), sodium chloride (75% RH), and potassium chloride (85% RH) were the salts used to control the relative humidity of each chamber. For film degradation testing, perovskite films were analyzed with X-ray diffraction on a Scintag XDS2000 XRD with a copper Kα source, UV-Vis absorption spectroscopy on a Perkin Elmer LAMBDA 1050 spectrophotometer, and X-ray Photoelectron Spectroscopy (XPS) on a Thermo Scientific ESCALAB 250Xi at regular intervals. For film degradation testing under 43% RH, we prepared the perovskite polymer hybrid films with greater thickness (310nm) than the control (170 nm) in order to obtain higher signal intensity for the polymer perovskite hybrid films in XRD. Under 85% RH, we matched the thickness of all 4 films to that of the control (170nm). Because different polymers changed the viscosity of the spin-coating solution, we had to optimize our perovskite and polymer concentrations to compare films with similar polymer content and thickness. Solar cells were degraded under 43% RH and fluorescent indoor lighting by placing them ~30 cm from a fluorescent lamp with 4100 K color temperature. We estimated the intensity of this illumination to be 0.5% as intense as incident solar illumination by using a photodiode to compare the intensity of our solar simulator illumination to the conditions under the fluorescent lamp.

Results and Discussion

Active layer morphology

In accordance with previous work on the incorporation of neutral polymer (PEG and PVP) into PSC active layers,[23,24,25] we observed using AFM, XRD, and SEM that introduction of a polymer with an acidic functional group, PAA, changes the active layer morphology (Figure 1). All three characterization techniques show that mixing PAA into the active layer leads to a decrease in crystallite size in thin films. The AFM data (figure 1 a,b) indicate a reduction in crystallite size along with a reduced roughness in the films. Comparing the XRD patterns (figure 1 c,d) reveals a slight broadening of the crystalline peaks, consistent with a smaller crystallite size. More importantly, the XRD data indicate that the crystal structure of the perovskite is preserved upon the addition of polymer. This result suggests that PAA phase separates from the perovskite without disrupting its crystal structure when a significant volume fraction (~20%) of polymer is incorporated into the film. SEM images of the films (figure 1 e,f) show a smaller domain size as well, consistent with our AFM data.

TEM can reveal nanoscale structural details in the perovskite-polymer hybrid films. The $MAPbI_3$ crystals rapidly degrade to PbI_2 under electron beam illumination, but these PbI_2 domains still show dark regions of contrast in the TEM. To our knowledge, only one of the previous studies on a perovskite polymer hybrid ($MAPbI_3$-PEG) included TEM data,[23] and so here we compare several different hybrids under the same preparation conditions to observe differences in crystal size and faceting. Figure 2 shows the differences in morphology that different polymer additives cause in the perovskite grains. We observe a mostly faceted crystal structure in the $MAPbI_3$ crystals in the absence of polymer, however, when we add PAA to the precursor solutions the individual crystals exhibit a more rounded morphology. We hypothesize

that change in perovskite grain faceting behavior in perovskite-polymer hybrid films is a consequence of polymer adhering to the perovskite grains as they grow. When we increase the concentration of polymer in these samples, the crystal size of the perovskites is decreased significantly for both $MAPbI_3$-PAA and $MAPbI_3$-polyethyleneimine (PEI). As an extreme example, at a 7:1 perovskite/polymer ratio by mass, PEI entirely prevents crystallization of perovskite in the film. When polyethylene glycol (PEG) is added, the faceted grain shape is mostly unaffected, however, as we have observed through XRD and AFM measurements, the domain size is smaller than the control $MAPbI_3$. These observations in $MAPbI_3$-PEG hybrids suggest that the interaction between PEG and the perovskite grains is different from that in PAA or PEI hybrid films. Our TEM characterization shows that differences in polymer composition can result in differences in perovskite grain faceting. These differences have the potential to affect the interconnectivity of perovskite grains within the active layer of PV devices. More rounded grains would tend to have less interfacial area to contact neighboring grains, and the grain size in these hybrid films is small enough that interconnectivity of the grains through the thickness of the film will affect device performance.

With respect to phase contrast, the polymer phase can be observed in some instances by TEM, but it is often hard to visualize it compared to the higher-z $MAPbI_3$ phase. We have included micrographs showing polymer domains within very thin hybrid perovskite–polymer samples in the supporting information (SI figure 1). These micrographs clearly show narrow polymer domains spanning the gap between much darker perovskite grains. However, TEM has not consistently or easily shown phase contrast in these materials because the preparation method for TEM samples (drop-casting) does not lead to samples with reproducible thickness.

To overcome the limitations of TEM characterization, nanomechanical AFM can be used to map the local modulus and adhesion forces in perovskite-polymer hybrid films to demonstrate phase separation because the elastic modulus of perovskite (~14 GPa)[42] is significantly higher than that of the polymers studied (figure 3). With nanomechanical AFM, we observed that $MAPbI_3$ perovskite films have a faceted grain structure, while the $MAPbI_3$-PAA hybrid films have smaller grains with softer structures present at the grain boundaries. In the control sample, the $MAPbI_3$ has a stepped structure on many of the grain surfaces, and the AFM tip adheres to a varying degree to these surfaces. This adhesion contrast is likely due to surface charges at the stepped surface of the crystal interacting with the silicon nitride AFM cantilever. To compare the mechanical properties at the grain boundaries, we have included line scans over these regions as a Supporting Information figure (SI figure 2). The grain boundaries in the $MAPbI_3$ control sample are softer than the crystal faces, but they do not show an increase in adhesion compared to the bulk of the crystal. In contrast, the micrographs of the $MAPbI_3$-PAA hybrid film indicate that the grain boundary regions appear softer and adhere to the tip significantly more than the surrounding grains (figure 3 d-f). This morphology indicates that perovskite grains nucleate and grow while the PAA polymer fills space in between the grains of the material. When we examined neat polymer films (without $MAPbI_3$) using this technique, we observed significantly more adhesion to the AFM tip than the perovskite films (SI figure 3). Thus, we conclude that the local increase in adhesion to the AFM tip combined with the observed decrease in modulus relative to the surrounding area indicates that polymer is present at the grain boundaries.

This result for $MAPbI_3$-PAA films can be compared with those for $MAPbI_3$-PEG and $MAPbI_3$-PVP films (SI figure 4). The $MAPbI_3$-PEG sample shows more faceted grains than the $MAPbI_3$-PAA sample, but the phase separation between the perovskite and polymer is similar to

what we observed for the $MAPbI_3$-PAA sample. The grain boundary regions adhere to the AFM tip strongly which indicates that the perovskite and PEG are phase-separated. The $MAPbI_3$-PVP sample is interesting in that we see what appears to be a three-phase mixture in the nanoscale morphology. We see larger, rectangular-shaped grains that have preferential faceting, and we see smaller rounded grains mixed intimately with the polymer phase. This morphology indicates that the spun-coat film undergoes initial phase separation between perovskite-rich phase and PVP-rich phase, followed by crystallization of perovskite in both phases which in turn leads to larger crystals in the perovskite-rich phase and small, PVP-embedded crystals in the PVP-rich phase. These results demonstrate that the microstructure of the perovskite-polymer hybrid film very much depends on the nature of the polymer used.

Film stability and intermolecular interactions

In order to experimentally simulate to some extent operating conditions that would be relevant to photovoltaic devices, we tested the stability of perovskite-polymer hybrid films under illumination in a humid environment. At 100% RH in air, both perovskite and perovskite-polymer hybrid films continuously absorb water from the atmosphere and degrade fully within 24 hours. However, at lower relative humidity levels, there are significant differences in the degradation rates of the pure perovskite and perovskite polymer hybrid films. We tested perovskite polymer hybrid film stability at 85% RH and 43% RH under ambient illumination (see figure 4 and SI figure 5). We examined $MAPbI_3$, $MAPbI_3$-PAA, $MAPbI_3$-PEG, and $MAPbI_3$-PVP at a 15:1 mass ratio of perovskite: polymer in the precursor solution and characterized their stability using XRD and XPS. At 43% relative humidity, the films degraded to PbI_2 slowly over the course of 3 weeks (SI figure 5). The control $MAPbI_3$ degraded within 10 days, while $MAPbI_3$-PEG and $MAPbI_3$-PVP degraded within 16 days, and finally the $MAPbI_3$-

PAA maintained some of its perovskite phase for 3 weeks. The accompanying XPS measurements showed no shift in the oxidation state of the Pb^{2+} over the course of the experiment, only a gradual reduction in the strength of the nitrogen signal as methylamine evaporated from the films. This contrasts with the results we found under 85% relative humidity (Figure 4). The general trend in stability is the same between the two humidity conditions: $MAPbI_3$-PAA is more stable than $MAPbI_3$-PEG and $MAPbI_3$-PVP which in turn are both more stable than the control $MAPbI_3$. However, the XRD for the 85% RH samples shows that the control $MAPbI_3$ film undergoes a phase transformation to a hydrate phase, and the presence of polymers appears to suppress this hydrate phase formation. This hydrate phase shows peaks in the XRD data at $2\theta = 8.5$ and 10.5 degrees which match those recently reported for the hydrate phase $(MA^+)_2(PbI_3^-)\cdot(H_2O)_2$.[16] This study[16] proposed that the hydrogen bonding ability of the solvent molecules, in this case water, affects the speed at which the hydrate phase is formed. Here, we observed that when polymer is present on the surface of the grains, the water-based hydrate phase $(MA^+)_2(PbI_3^-)\cdot(H_2O)_2$ is not formed. The evidence of degradation to a different phase implies that the degradation proceeds through a different mechanism when polymer is present at the crystal surface. The XPS spectra show that the Pb^{2+} is reduced to Pb^0 at 85% RH in the $MAPbI_3$-PVP sample, which is a phase transition that is not observed for the other samples. The reduction of Pb^{2+} to Pb^0 also implies that the $MAPbI_3$-PVP system follows a different degradation pathway than the other $MAPbI_3$-polymer systems. PVP acts as a surface stabilizer, growth modifier, and reducing agent in the field of nanoparticle synthesis,[43] and thus, this XPS data suggests that it is interacting with the surface of the $MAPbI_3$ crystals in a similar fashion leading to a reduction of the Pb^{2+} to Pb^0 during the degradation of the perovskite.

To explain our observations of differences in stability between the perovskite control and the various perovskite-polymer hybrid thin films, we focused on chemical differences among the polymers used. Based on the previous hypothesis proposed for the $MAPbI_3$-PEG hybrid,[23] water absorption experiments on the polymers were performed to investigate if there was any correlation between absorption and stability. We found that while different polymers absorbed significantly different amounts of water in humid conditions, these differences did not correlate to our film stability observations (SI figure 6). Next, we performed FT-IR experiments to characterize chemical interactions at the surface of $MAPbI_3$-polymer powders (we have included the FT-IR data in SI figure 7). We observed that in the case of PVP, the carbonyl stretch peak at 1633 cm^{-1} became narrower in width with a slight shift to a lower wavenumber for PVP suggesting proton-accepting hydrogen bond formation.[24] The narrowing of the carbonyl peak was also observed in PAA at 1710 cm^{-1}, but a noticeable shift was not observed. Due to the broad nature of the peaks and peak overlaps between perovskites and polymers in the range of 2500-3500 cm^{-1} where O-H stretching bands are typically observed, it was determined that different techniques are necessary to further investigate the intermolecular interactions involved. Thus, to explain the differences in stability between the various $MAPbI_3$-polymer systems, we carried out a more thorough investigation of chemical stability using NMR spectroscopy and single crystal growth to better understand the mechanism for increased film stability.

To probe the interaction between the polymers and the perovskite precursors in solution, we performed NMR experiments in an environment that simulates the casting solution. Figure 5 shows a series of NMR spectra of the $MAPbI_3$ precursor solution and $MAPbI_3$-polymer precursor solutions in DMSO-d_6. The peak at 7.23 ppm, corresponding to the ammonium protons, shifts downfield and sharpens upon addition of acidic polymers such as poly(glutamic

acid) (PGA) or PAA, remains at the same position upon addition of neutral polymers such as PEG or PVP, and shifts upfield upon addition of basic polymers such as polyethyleneimine. Additionally, SI figure 8 shows a corresponding broadening and upfield shift of the carboxylic acid protons on PAA when mixed with $MAPbI_3$ precursor solution. This trend points to acid-base type interactions between MAI and the ionizable group of each polymer. We note that we did not observe a strong interaction between methylammonium iodide and PEG, as claimed in a previous study,[23] possibly due to our careful control of water levels in the sample preparation such as vacuum oven drying and storage in a nitrogen-filled glovebox.

Acid-base interactions have previously been shown to have a significant impact on the crystallization and stability of perovskite thin films. It has been shown that the formation of perovskite hydrate phases is dependent on the hydrogen bond acceptor strength of the solvent[16] which is water in the case of atmospheric degradation. Our NMR data suggest that the hydrogen bonding ability of the methylammonium cations in solution are affected by the presence of polymers, and therefore we propose that these chemical interactions are important to the stability of the perovskite phase. As an analogous example, $MAPbI_3$ films are particularly unstable on ZnO surfaces because the basic ZnO surface deprotonates the methylammonium leading to rapid degradation.[44] Acidic oxides such as TiO_2 are more compatible with the crystallization of $MAPbI_3$, and so the increased stability we observe with acid-functionalized polymers is consistent with these previous studies. Therefore, based on our film stability experiments and NMR observations, we propose that the proton-donating hydrogen bonding ability of the PAA to the MAI, in contrast to PVP and PEG, competes with the ability of atmospheric water vapor to bond to the MAI and form the perovskite hydrate phase $(MA^+)_2(PbI_3^-)\cdot(H_2O)_2$, resulting in the blocking of the perovskite degradation pathway and film stability.

While NMR captures some of the interactions between these species in solution, there are also chemical interactions between the surface of the crystal and the polymer species that affect crystal formation and thin film morphology. To characterize these differences, we grew crystals *via* solvent vapor diffusion of $MAPbI_3$ with PAA, PEG, and PVP dissolved in the crystallization solution (Figure 6). When the crystals are grown with polymer present, the crystal growth rate is slowed compared to the $MAPbI_3$ control leading to smaller crystal sizes. $MAPbI_3$ crystals without polymer exhibit a mixture of (100)-type and (110)-type faceting. The $MAPbI_3$-PEG hybrid shows preference for (110)-type faceting leading to an elongated dodecahedron morphology. $MAPbI_3$-PAA and $MAPbI_3$-PVP grow with mainly (100)-type faceting and appear cuboid-shaped, although the $MAPbI_3$-PVP crystals are less faceted overall. The differences in faceting between the various polymers are likely due to differences in polymer adhesion to and interaction with the growing crystal faces. We hypothesize that neutral polymers such as PEG would tend to adhere to more neutral crystal faces, while polymers with polar interactions with the $MAPbI_3$ such as PAA and PVP would tend to adhere to more charged crystal faces. We have included atomic models of the $MAPbI_3$ cut along the (100) and (110) planes (see SI Figure 9). When the crystal is truncated along (110)-type planes, the resulting crystal face is either positively charged (a higher concentration of Pb^{2+} and MA^+ compared to I^-) or entirely negatively charged (I^-). When the crystal is truncated along (100)-type planes, however, the growth is significantly closer to being charge neutral because (100)-type crystal truncations have a mixture of positively and negatively charged species. Thus, as the crystals grow, polymers with polar interactions to the perovskite, PAA and PVP, would tend to adhere to charged crystal faces such as (110)-type planes and slow those growth directions. Similarly, polymers lacking polar interactions with the perovskite such as PEG would tend to adhere to more neutral crystal faces

such as (100)-type planes while allowing the (110)-type planes to grow. If we re-examine the morphology of our perovskite-polymer thin films considering our observations on the single crystal growth we can explain more of the structural features present. First, we observe that in the $MAPbI_3$-PVP sample, one of the phases present in that film is a cuboid-like structure. Second, we observed a higher amount of faceting on the $MAPbI_3$-PEG samples in TEM which is consistent with what we observe in the single crystal growth. These two observations indicate that at least some of the chemical interactions we have observed in the single crystal growth and NMR studies can be used to explain the thin film morphology. Overall, using both microscopy and spectroscopic techniques, we have demonstrated that chemical interactions between the perovskite precursors and polymers affect the hybrid film morphology and degradation pathway.

Photovoltaic performance and stability

The goal of adding polymers to the active layer of the perovskite solar cell is to increase the stability of devices. We designed these devices so that the interlayers and contacts last longer than the active layer under conditions known to lead to degradation. Typical hole transport materials (HTMs), such as Spiro-OMeTAD and polytriarylamine, are not compatible with long term device stability, since the additives used on these HTMs to increase hole mobility and improve wetting properties (4-*tert*-butyl pyridine and lithium bis(trifluoromethane)sulfonamide) tend to dissolve and oxidize the perovskite active layer.[45] Therefore, we designed our devices with an ITO transparent contact, PEDOT:PSS hole transport layer, perovskite active layer, [6,6]-phenyl-C61-butyric acid methyl ester ($PC_{61}BM$) electron transport layer, bathocuproine (BCP) exciton blocking layer, and gold counter electrode (SI figure 10). We chose gold as the counter electrode material because as the active layer decomposes, the released iodine can react with a silver or aluminum counter electrode in the presence of humidity, corroding the device contact.

We then proceeded to optimize device performance for the control devices and for the perovskite polymer hybrid devices.

Representative J-V curves for $MAPbI_3$ and perovskite-polymer hybrid solar cells are included in the supporting information (SI figure 11). $MAPbI_3$-PVP devices exhibit significantly lower efficiency consistent with their smaller crystal size and the previous report on their photovoltaic performance.[24] $MAPbI_3$-PEG devices exhibited high current values and a higher amount of hysteresis than the other devices, and this behavior is also somewhat consistent with the previous report on $MAPbI_3$-PEG.[23] Device stability tests were therefore performed on $MAPbI_3$ and $MAPbI_3$-PAA because our data shows that $MAPbI_3$-PAA films have reasonable efficiency, low hysteresis, and the highest stability in our film stability tests.

Optimized PSC and polymer hybrid PSC device performance and stability over time are plotted in figure 7. We exposed the cells to a controlled air environment with 43% relative humidity under ambient indoor illumination. The inclusion of PAA into the active layer reduces the peak power conversion efficiency (PCE) of the solar cells from 13% in pure PSCs to 9% in PAA hybrid PSCs, but increases their longevity significantly. The pure PSCs lose 50% of their original PCE within 24 hours, and they degrade to significantly less than 1% efficiency within 2 days. The PAA hybrid PSCs, however, retain their initial PCE for 3 days and slowly degrade to 50% of their original efficiency over 8 days. The device stability results under illumination are consistent with the film stability results that we obtained, showing that devices incorporating PAA into the active layer increase their long-term stability under humidity and illumination. We then compared $MAPbI_3$ devices to 20:1 $MAPbI_3$-PAA devices aged in the dark at 43% relative humidity for two weeks (SI figure 12). We find that the $MAPbI_3$ devices have an initial 6-day period of stable PCE followed by a moderate decline in efficiency over the next 8 days. The 20:1

$MAPbI_3$-PAA devices degrade at a slower but steady rate starting from day 1, and so they degrade in about the same amount of time as the $MAPbI_3$ devices.

The initial stability of the control devices can be explained by changes in the stoichiometry of the perovskite grain boundaries. It has been reported that slight excesses of PbI_2 in the grain boundaries can be beneficial to the open circuit voltage and J_{sc}.[46] Thus, as the devices start to degrade, the initially stoichiometric mixture becomes slightly PbI_2 rich, which is beneficial to the overall performance. PbI_2 has been shown to passivate the surface of $MAPbI_3$ grains which suppresses charge recombination.[47] However, as a bulk phase PbI_2 has significantly poorer charge transport properties than those of the perovskite.[48] Therefore, as degradation progresses, excess PbI_2 accumulates further and rapidly reduces the efficiency of the devices. When we consider that the grain boundaries of the $MAPbI_3$-PAA films are coated with polymer instead of PbI_2, it is likely that local changes in stoichiometry at the grain boundaries are not possible. Instead, the $MAPbI_3$-PAA devices degrade at a slower, but steady rate. It remains surprising that the 20:1 $MAPbI_3$-PAA devices degraded as quickly as the $MAPbI_3$ devices in dark and humid conditions because our film stability experiments showed that the $MAPbI_3$ film degrades more quickly than the $MAPbI_3$-PAA film. However, those experiments characterize only the bulk degradation rate and do not measure degradation at the interface between the perovskite and surrounding layers. In PSCs, degradation of the interface of the active layer with the transport layers is sufficient to degrade device performance. We observed that at the 14-day time point under dark and humid conditions, both the control and PAA-hybrid PSCs still appear to have a brown color. Thus, the interfaces of these films with their contact layers must have degraded over time.

To mitigate the negative effects of reduced grain size on device performance in experimental devices, we took steps to increase the size of our perovskite grains. We have increased grain size in these films by increasing annealing temperature to 120°C as well as changing the spin-coating solvent mixture to a DMF/DMSO mixture for our experimental devices (SI figure 13). One of the challenges associated with creating hybrid perovskite-polymer devices is the reduction in short circuit current density (J_{sc}) and fill factor (FF) for these devices. Whereas the control $MAPbI_3$ devices had J_{sc}~18 mA/cm^2 and FF= 0.75, even under our best-optimized conditions, devices with PAA had J_{sc}~15 mA/cm^2 and FF= 0.65. The changes in processing conditions that we used to increase grain size significantly improved the photovoltaic performance of the $MAPbI_3$-PAA hybrid PSCs, and these optimized devices demonstrated a significant improvement in stability compared to the control under humidity and illumination.

To investigate the effect of a polymer phase in the active layer on carrier lifetime we performed steady-state and time-resolved photoluminescence (TR-PL) experiments on our perovskite-polymer hybrid films. The steady-state PL emission shows that $MAPbI_3$, $MAPbI_3$-PAA and $MAPbI_3$-PEG have emission maxima between 760 and 770 nm while $MAPbI_3$-PVP has a maximum near 730 nm (SI figure 14). In the TR-PL experiment, we observed that $MAPbI_3$-PAA and $MAPbI_3$-PEG samples have a longer PL lifetime compared to the $MAPbI_3$ control (SI figure 15). With respect to $MAPbI_3$ -PVP, there is a PL decay process comparable to the $MAPbI_3$-PAA and $MAPbI_3$-PEG samples at ~730 nm (<10ns) and a much slower decay process (42 ns) that can be observed at ~765 nm (SI figure 16). This red-shift in PL is unique to the $MAPbI_3$-PVP sample, and it may be a result of the two distinct perovskite phases we found in the morphological study leading to different carrier decay processes. Carrier lifetime in these films can be affected by crystallinity of the perovskite phase, and we observed that the $MAPbI_3$-

PVP film has the lowest crystallinity of the samples tested. Our TR-PL results are generally consistent with the trend of higher PL lifetime in polymer-containing films than in the control $MAPbI_3$ films observed in previous work on TR-PL in perovskite-polymer hybrids.[38] In that study, higher PL lifetime was attributed to a reduction in the nonradiative recombination rate in the polymer-containing samples.[38]

From our TR-PL result, we therefore attribute the lower fill-factor in hybrid perovskite-polymer devices to increased series resistance in the device rather than reduced carrier lifetime because the PL lifetime is not decreased in the hybrid films. The added series resistance can be attributed to smaller grain sizes necessitating charge transport across many more grain boundaries through the thickness of the device. This effect can be somewhat mitigated by making a thinner active layer. Adding less polymer to the system can also improve the initial electronic performance, as demonstrated previously,[38] but from our own observations, adding less polymer to the active layer reduces the longevity added to the device. This trade-off between performance and stability needs to be considered in the design of any future perovskite-polymer hybrid solar cells. It remains to be seen if the device processing approaches shown in other work to produce significantly larger grain sizes and high-performance devices[38] can be combined with our observation that the acidic functionality of PAA tends to increase film stability the most under humid and illuminated conditions. Overall, the inclusion of PAA into PSCs tends to greatly increase the stability of the device under illuminated conditions at the expense of a modest amount of its starting efficiency.

Conclusions

We have demonstrated that incorporation of PAA, PEG, and PVP into the active layer of perovskite solar cells causes changes to the faceting of the perovskite grains and improves stability by changing the degradation pathway. These changes in morphology and stability are the result of acid-base interactions between the polymer functional groups and methylammonium in the perovskite. Utilizing these observations, we have demonstrated significant improvements in device stability under humid, illuminated conditions in $MAPbI_3$-PAA hybrid PSCs. We envision that this study provides insights into rationally designing polymer additives with multiple functionalities such as ultraviolet protection, water vapor permeation barrier, or charge transport, towards more reliable hybrid perovskite-organic solar cells.

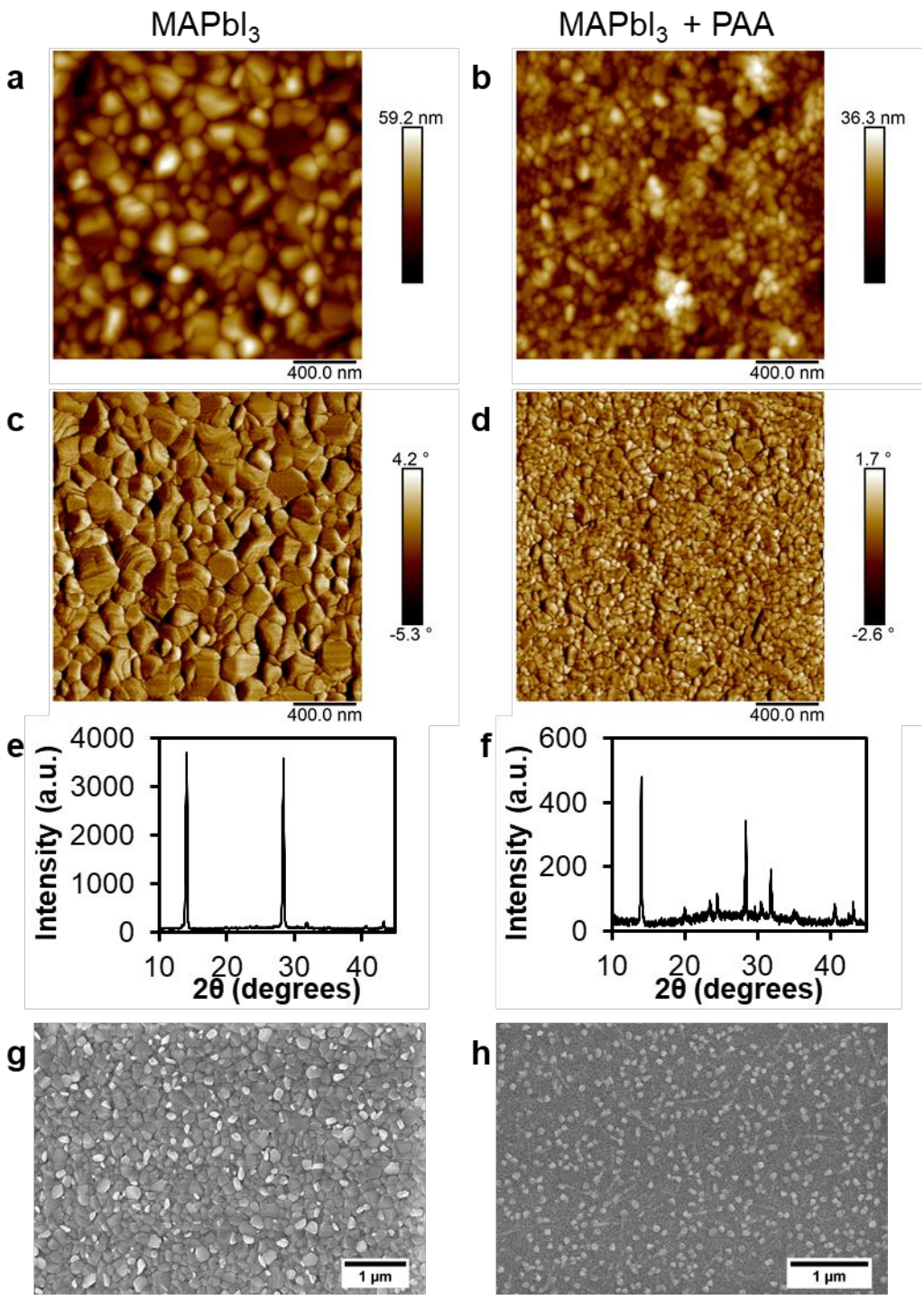

Figure 1. Comparison of perovskite grain structures with and without polymer additives. AFM height a), b), phase c), d), XRD e), f), and SEM g), h) of $MAPbI_3$ perovskite and $MAPbI_3$ perovskite mixed with poly(acrylic acid). All 3 techniques show a reduction in grain size without showing contrast between polymer and perovskite domains.

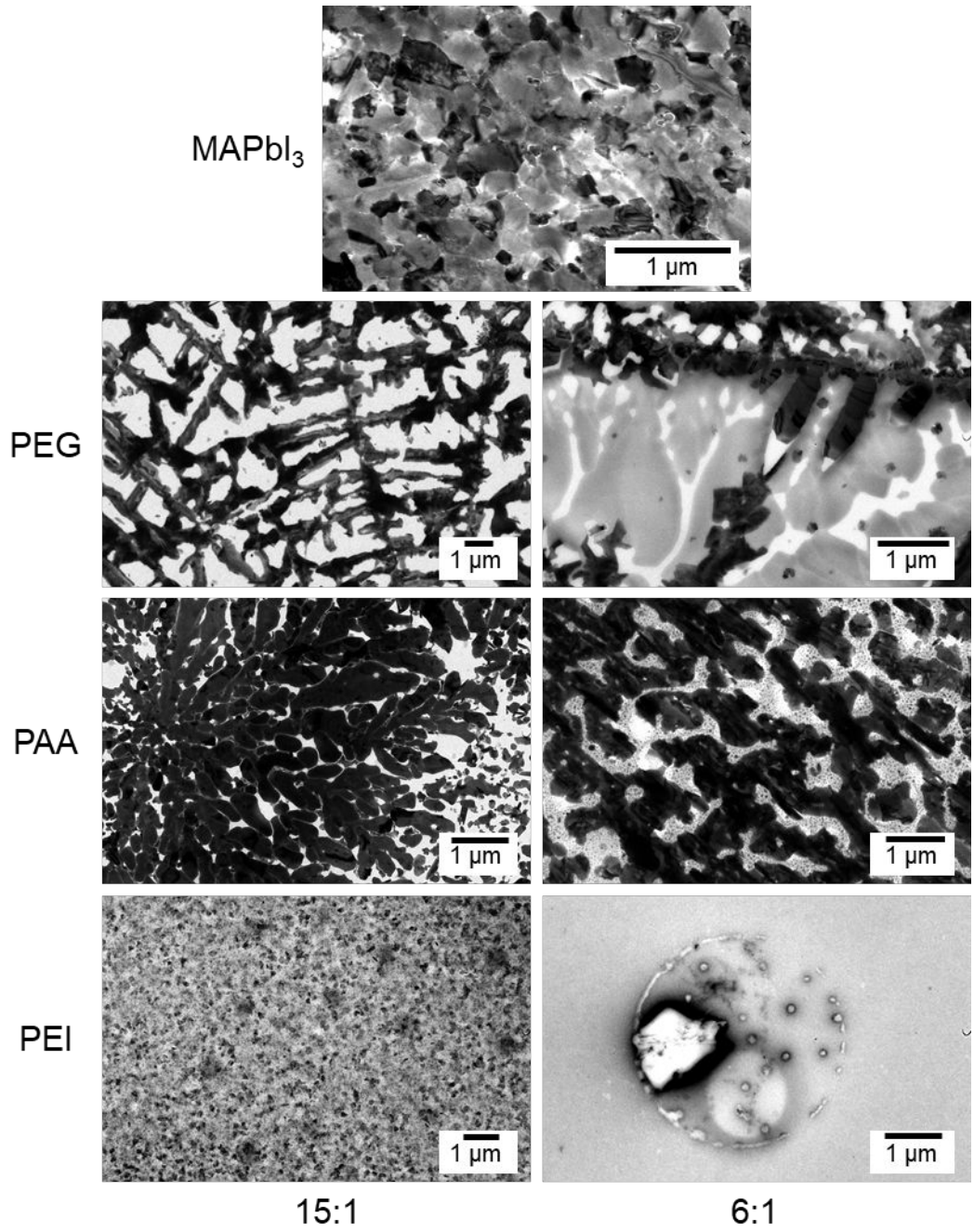

Figure 2. TEM images of drop-cast perovskite and perovskite/polymer hybrid films. Left column samples have mass ratios of perovskite to polymer of 15:1, while right column samples have 6:1. As we go down the columns, the crystal size gets smaller and the crystallization becomes more disrupted by the presence of polymer.

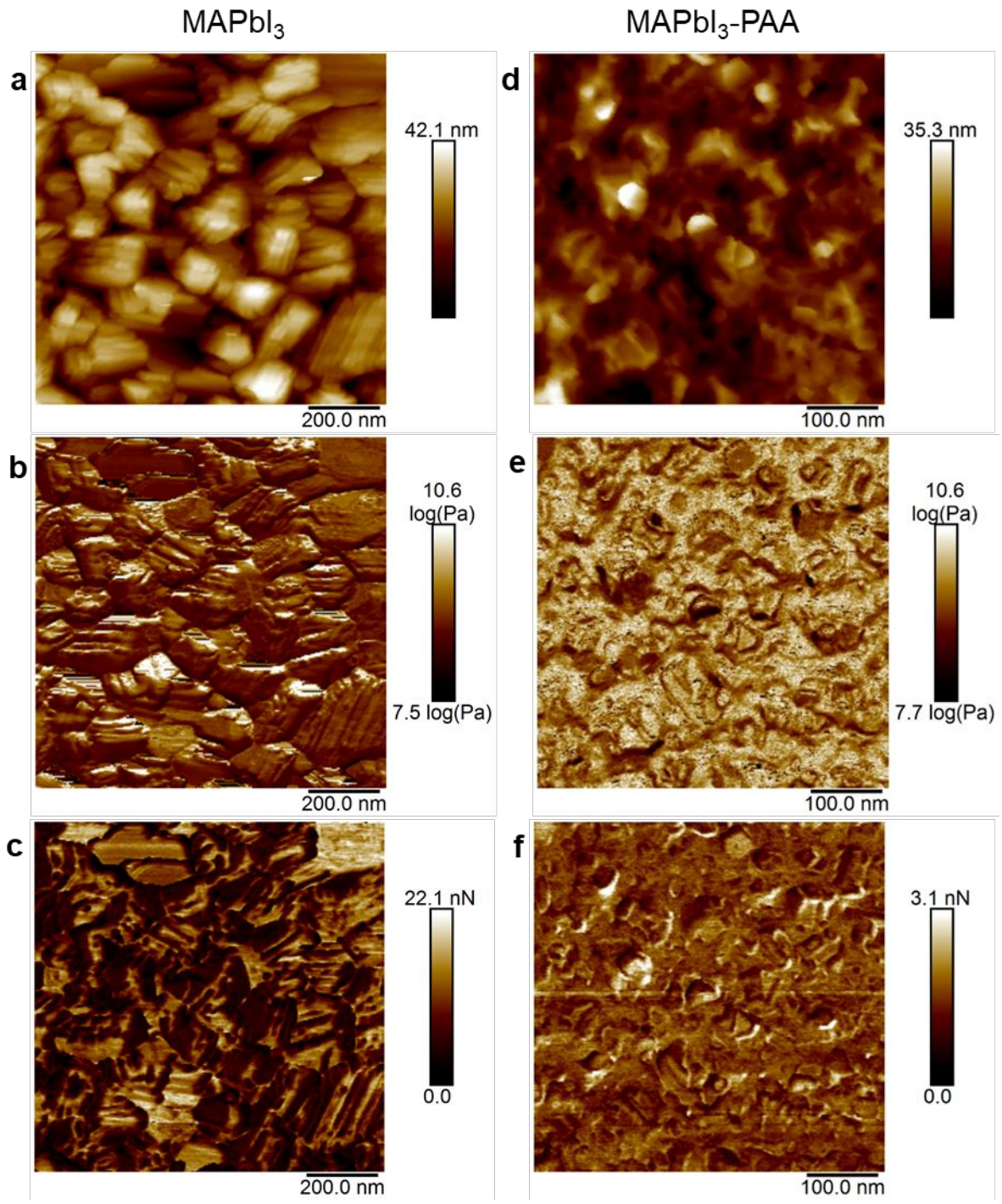

Figure 3. AFM height (a,d), log(DMT modulus) (b,e), and adhesion (c,f) micrographs of $MAPbI_3$ (a-c) and 15:1 mass ratio $MAPbI_3$-PAA (d-f).

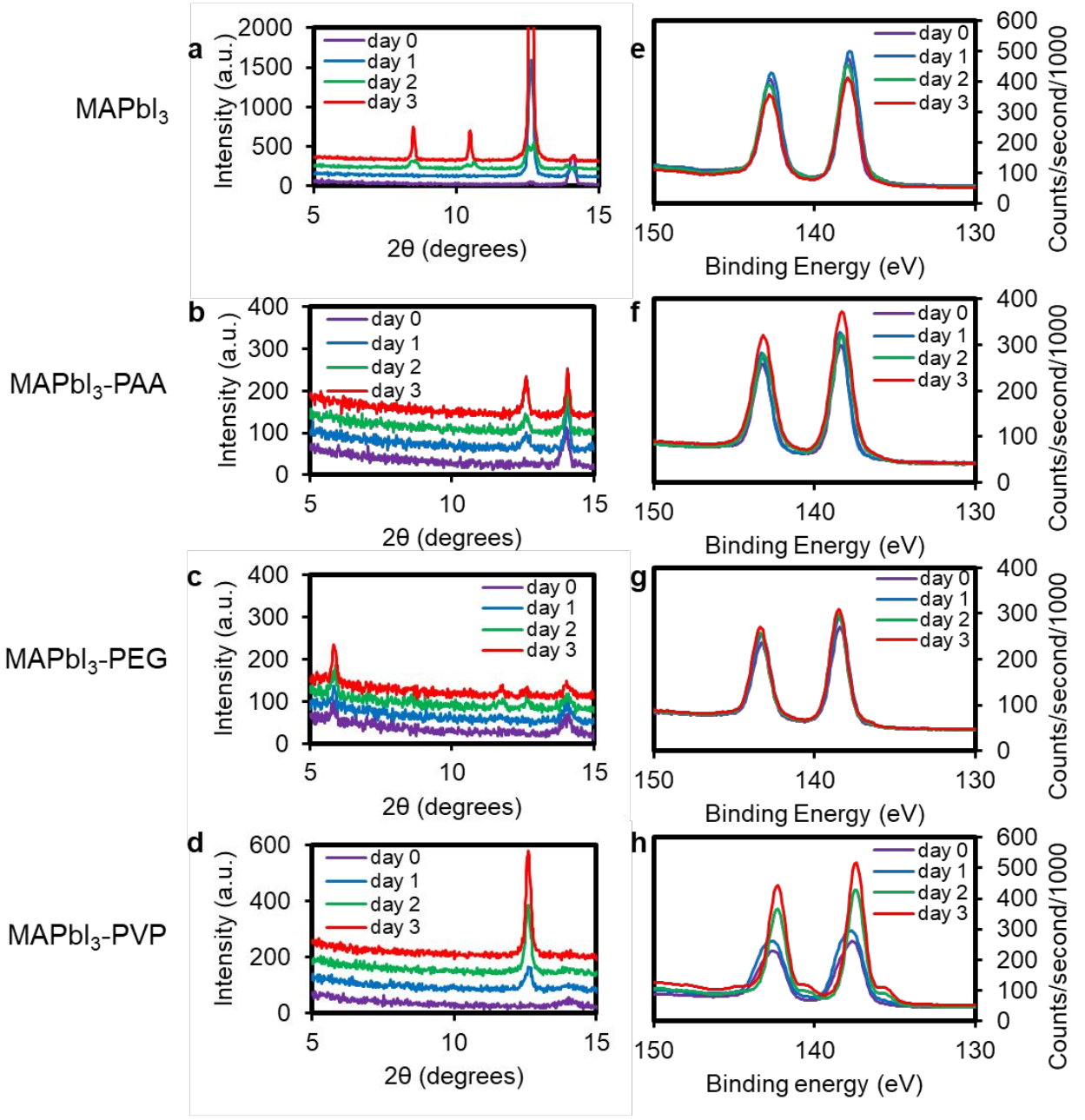

Figure 4. XRD (a-d) and XPS (e-h) of $MAPbI_3$ and $MAPbI_3$-polymer hybrid films aged at 85%RH under illumination. The new peaks appearing in the XRD of the $MAPbI_3$ sample at 8.5 and 10.5 degrees correspond to $(MA^+)_2(PbI_3^-)\cdot(H_2O)_2$ hydrate phase formation. The new peaks appearing in the XPS data for the $MAPbI_3$-PVP sample correspond to Pb^0.

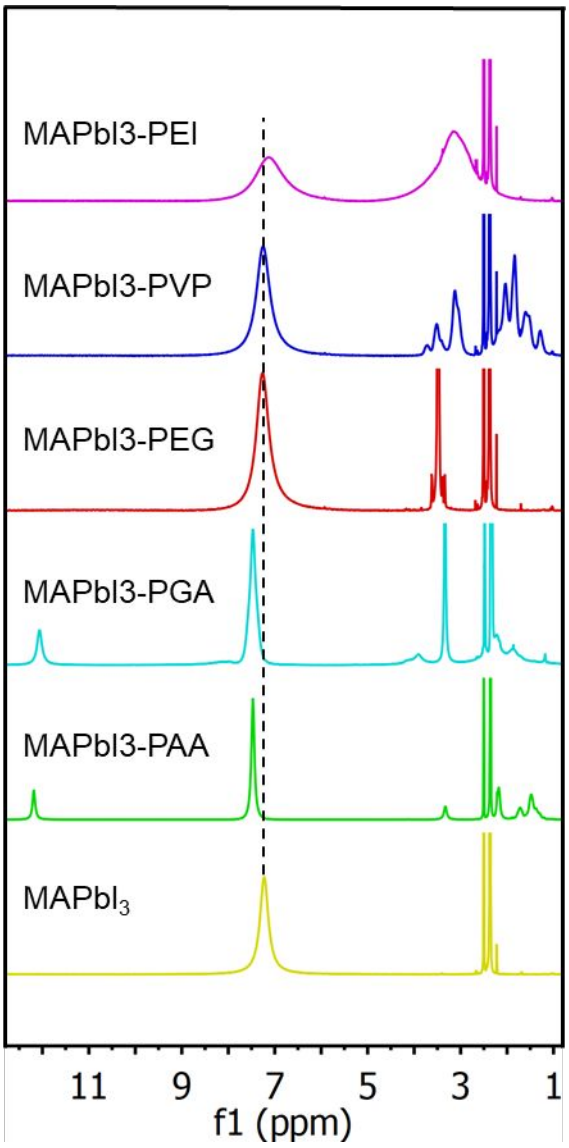

Figure 5. NMR spectra of the perovskite precursor solution and perovskite/polymer precursor solutions in DMSO-d_6. The peak at 7.23 ppm, corresponding to the ammonium protons, shifts downfield and sharpens upon addition of acidic polymers such as polyglutamic acid or polyacrylic acid, remains at the same position upon addition of neutral polymers such as poly(ethylene oxide) or polyvinylpyrrolidone, and shifts upfield upon addition of basic polymers such as polyethyleneimine.

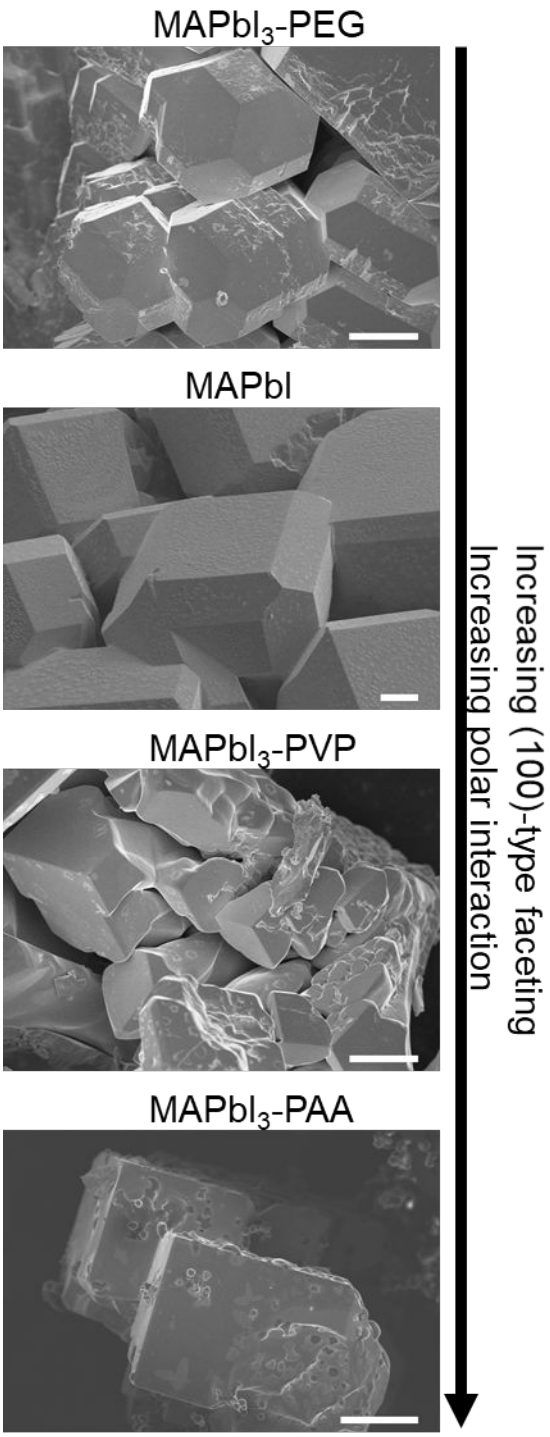

Figure 6. Single crystal growth of $MAPbI_3$ with various polymers added to the crystallization solution. $MAPbI_3$ alone exhibits a mixture of (100)-type and (110)-type faceting. $MAPbI_3$-PEG shows preference for (110)-type faceting leading to an elongated dodecahedron morphology. $MAPbI_3$-PAA and $MAPbI_3$-PVP grow mainly (100)-type faceting, although the $MAPbI_3$-PVP crystals are less faceted overall. (Scale bar: 50 μm)

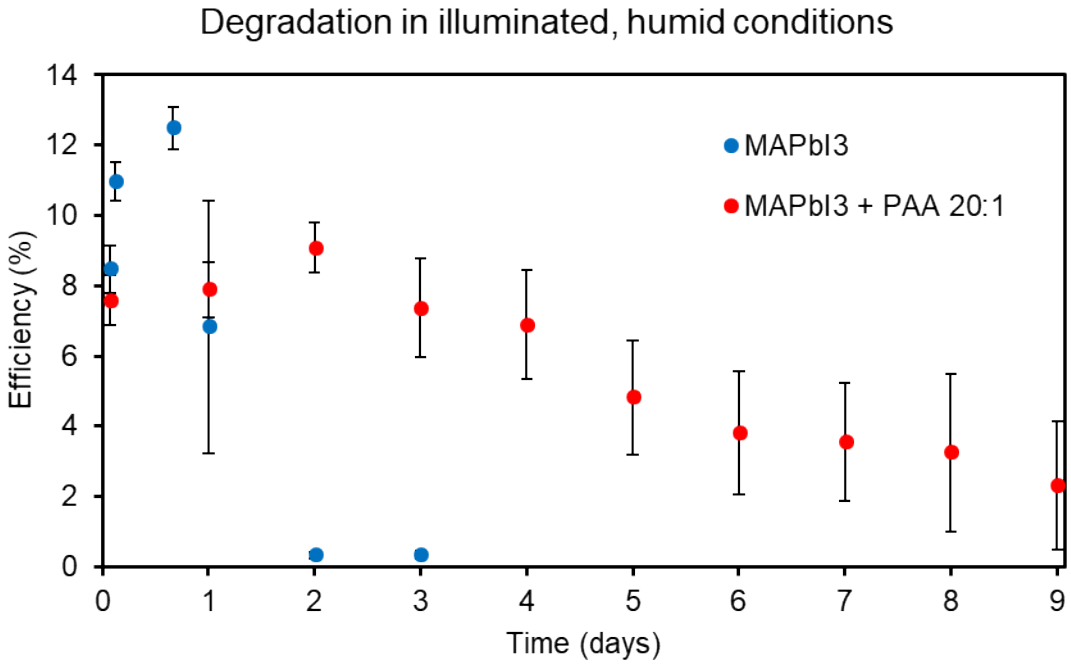

Figure 7. Perovskite solar cell stability over time under 43% relative humidity in air with illumination. Error bars indicate standard deviation across n=7 devices.

Acknowledgements

This work was supported by the U.S. Department of Energy, Office of Science, Basic Energy Sciences, under Awards DE- FG02-00ER45810 (S.I.S.) and DE-FG02-99ER14999 (M.R.W.). This work made use of the EPIC, Keck-II, and SPID facilities of Northwestern University's NU*ANCE* Center, which has received support from the Soft and Hybrid Nanotechnology Experimental (SHyNE) Resource (NSF ECCS-1542205); the MRSEC program (DMR-1720139) at the Materials Research Center; the International Institute for Nanotechnology (IIN); the Keck Foundation; and the State of Illinois, through the IIN. This work made use of the J. B.Cohen X-Ray Diffraction Facility supported by the MRSEC program of the National Science Foundation (DMR-1720139) at the Materials Research Center of Northwestern University. This work made use of the IMSERC at Northwestern University, which has received support from the Soft and Hybrid Nanotechnology Experimental (SHyNE) Resource (NSF ECCS-1542205); the State of Illinois and International Institute for Nanotechnology (IIN). The authors thank Karen Qu for her contribution to preliminary spin casting experiments of the perovskite-polymer hybrid thin films.

References

(1) Dong, Q.; Fang, Y.; Shao, Y.; Mulligan, P.; Qiu, J.; Cao, L.; Huang, J. Electron-Hole Diffusion Lengths > 175 Mm in Solution-Grown CH3NH3PbI3single Crystals. *Science.* **2015**, *347* (6225), 967–970.

(2) Leijtens, T.; Stranks, S. D.; Eperon, G. E.; Lindblad, R.; Johansson, E. M. J.; McPherson, I. J.; Rensmo, H.; Ball, J. M.; Lee, M. M.; Snaith, H. J. Electronic Properties of Meso-Superstructured and Planar Organometal Halide Perovskite Films: Charge Trapping, Photodoping, and Carrier Mobility. *ACS Nano* **2014**, *8* (7), 7147–7155.

(3) Green, M. A.; Ho-Baillie, A.; Snaith, H. J. The Emergence of Perovskite Solar Cells. *Nat Phot.* **2014**, *8* (7), 506–514.

(4) Manser, J. S.; Kamat, P. V. Band Filling with Free Charge Carriers in Organometal Halide Perovskites. *Nat. Photonics* **2014**, *8* (9), 737–743.

(5) Zhao, T.; Shi, W.; Xi, J.; Wang, D.; Shuai, Z. Intrinsic and Extrinsic Charge Transport in CH3NH3PbI3 Perovskites Predicted from First-Principles. *Sci. Rep.* **2016**, *7* (December 2015), 19968.

(6) Kojima, A.; Teshima, K.; Shirai, Y.; Miyasaka, T. Organometal Halide Perovskites as Visible-Light Sensitizers for Photovoltaic Cells. *J. Am. Chem. Soc.* **2009**, *131* (17), 6050–6051.

(7) Yang, W. S.; Park, B.-W.; Jung, E. H.; Jeon, N. J. Iodide Management in Formamidinium-Lead-Halide – Based Perovskite Layers for Efficient Solar Cells. *Science.* **2017**, *356* (6345), 1376–1379.

(8) Lee, M. M.; Teuscher, J.; Miyasaka, T.; Murakami, T. N.; Snaith, H. J. Efficient Hybrid Solar Cells Based on Meso-Superstructured Organometal Halide Perovskites. *Science.* **2012**, *338* (November), 643–647.

(9) Burschka, J.; Pellet, N.; Moon, S.-J.; Humphry-Baker, R.; Gao, P.; Nazeeruddin, M. K.; Grätzel, M. Sequential Deposition as a Route to High-Performance Perovskite-Sensitized Solar Cells. *Nature* **2013**, *499* (7458), 316–320.

(10) Ball, J. M.; Lee, M. M.; Hey, A.; Snaith, H. J. Low-Temperature Processed Meso-Superstructured to Thin-Film Perovskite Solar Cells. *Energy Environ. Sci.* **2013**, *6*, 1739.

(11) Malinkiewicz, O.; Yella, A.; Lee, Y. H.; Espallargas, G. M. M.; Graetzel, M.; Nazeeruddin, M. K.; Bolink, H. J. Perovskite Solar Cells Employing Organic Charge-Transport Layers. *Nat. Photonics* **2014**, *8* (2), 128–132.

(12) Li, Z.; Yang, M.; Park, J. S.; Wei, S. H.; Berry, J. J.; Zhu, K. Stabilizing Perovskite Structures by Tuning Tolerance Factor: Formation of Formamidinium and Cesium Lead Iodide Solid-State Alloys. *Chem. Mater.* **2016**, *28* (1), 284–292.

(13) Wang, Z.; Shi, Z.; Li, T.; Chen, Y.; Huang, W. Stability of Perovskite Solar Cells: A Prospective on the Substitution of the A Cation and X Anion. *Angew. Chemie Int. Ed.* **2016**, 2–25.

(14) Frost, J. M.; Butler, K. T.; Brivio, F.; Hendon, C. H.; van Schilfgaarde, M.; Walsh, A. Atomistic Origins of High-Performanc1. Frost, J. M. et Al. Atomistic Origins of High-Performance in Hybrid Halide Perovskite Solar Cells. Nano Lett. 14, 2584–90 (2014).e in Hybrid Halide Perovskite Solar Cells. *Nano Lett.* **2014**, *14* (5), 2584–2590.

(15) Jeon, N. J.; Noh, J. H.; Kim, Y. C.; Yang, W. S.; Ryu, S.; Seok, S. Il. Solvent Engineering for High-Performance Inorganic-Organic Hybrid Perovskite Solar Cells. *Nat. Mater.* **2014**, *13* (July), 1–7.

(16) Nakamura, E.; Shoyama, K.; Sato, W.; guo, Y. Effects of Water on the Forward and Backward Conversions of Lead(II) Iodide to Methylammonium Lead Perovskite. *J. Mater. Chem. A* **2017**.
(17) Bryant, D.; Aristidou, N.; Pont, S.; Sanchez-Molina, I.; Chotchunangatchaval, T.; Wheeler, S.; Durrant, J. R.; Haque, S. A. Light and Oxygen Induced Degradation Limits the Operational Stability of Methylammonium Lead Triiodide Perovskite Solar Cells. *Energy Environ. Sci.* **2016**.
(18) Saliba, M.; Matsui, T.; Seo, J.-Y.; Domanski, K.; Correa-Baena, J.-P.; Mohammad K., N.; Zakeeruddin, S. M.; Tress, W.; Abate, A.; Hagfeldt, A.; et al. Cesium-Containing Triple Cation Perovskite Solar Cells: Improved Stability, Reproducibility and High Efficiency. *Energy Environ. Sci.* **2016**, *9* (6), 1989–1997.
(19) Leijtens, T.; Eperon, G. E.; Pathak, S.; Abate, A.; Lee, M. M.; Snaith, H. J. Overcoming Ultraviolet Light Instability of Sensitized TiO_2 with Meso-Superstructured Organometal Tri-Halide Perovskite Solar Cells. *Nat. Commun.* **2013**, *4*, 2885.
(20) Li, X.; Dar, M. I.; Yi, C.; Luo, J.; Tschumi, M.; Zakeeruddin, S. M.; Nazeeruddin, M. K.; Han, H.; Grätzel, M. Improved Performance and Stability of Perovskite Solar Cells by Crystal Crosslinking with Alkylphosphonic Acid ω-Ammonium Chlorides. *Nat. Chem.* **2015**, *7* (August), 1–9.
(21) Song, X.; Wang, W.; Sun, P.; Ma, W.; Chen, Z. K. Additive to Regulate the Perovskite Crystal Film Growth in Planar Heterojunction Solar Cells. *Appl. Phys. Lett.* **2015**, *106* (3).
(22) Chueh, C. C.; Liao, C. Y.; Zuo, F.; Williams, S. T.; Liang, P. W.; Jen, A. K. Y. The Roles of Alkyl Halide Additives in Enhancing Perovskite Solar Cell Performance. *J. Mater. Chem. A* **2015**, *3* (17), 9058–9062.
(23) Zhao, Y.; Wei, J.; Li, H.; Yan, Y.; Zhou, W.; Yu, D.; Zhao, Q. A Polymer Scaffold for Self-Healing Perovskite Solar Cells. *Nat. Commun.* **2016**, *7*, 10228.
(24) Guo, Y.; Shoyama, K.; Sato, W.; Nakamura, E. Polymer Stabilization of Lead(II) Perovskite Cubic Nanocrystals for Semitransparent Solar Cells. *Adv. Energy Mater.* **2016**, *6* (6), 1–9.
(25) Xiang, W.; Chen, Q.; Wang, Y.; Liu, M.; Huang, F.; Bu, T.; Wang, T.; Cheng, Y.-B.; GONG, X.; Zhong, J.; et al. Improved Air Stability of Perovskite Hybrid Solar Cells via Blending Poly(Dimethylsiloxane)-Urea Copolymer. *J. Mater. Chem. A* **2017**, *00*, 1–9.
(26) Bi, D.; Yi, C.; Luo, J.; Décoppet, J. D.; Zhang, F.; Zakeeruddin, S. M.; Li, X.; Hagfeldt, A.; Grätzel, M. Polymer-Templated Nucleation and Crystal Growth of Perovskite Films for Solar Cells with Efficiency Greater than 21%. *Nat. Energy* **2016**, *1* (10), 1–5.
(27) Chang, C. Y.; Chu, C. Y.; Huang, Y. C.; Huang, C. W.; Chang, S. Y.; Chen, C. A.; Chao, C. Y.; Su, W. F. Tuning Perovskite Morphology by Polymer Additive for High Efficiency Solar Cell. *ACS Appl. Mater. Interfaces* **2015**, *7* (8), 4955–4961.
(28) Sun, C.; Guo, Y.; Fang, B.; Yang, J.; Qin, B.; Duan, H.; Chen, Y.; Li, H.; Liu, H. Enhanced Photovoltaic Performance of Perovskite Solar Cells Using Polymer P(VDF-TrFE) as a Processed Additive. *J. Phys. Chem. C* **2016**, *120* (24), 12980–12988.
(29) Dong, Q.; Wang, Z.; Zhang, K.; Yu, H.; Huang, P.; Liu, X.; Zhou, Y.; Chen, N.; Song, B. Easily Accessible Polymer Additives for Tuning the Crystal-Growth of Perovskite Thin-Films for Highly Efficient Solar Cells. *Nanoscale* **2016**, *8* (10), 5552–5558.
(30) Quan, L. N.; Yuan, M.; Comin, R.; Voznyy, O.; Beauregard, E. M.; Hoogland, S.; Buin, A.; Kirmani, A. R.; Zhao, K.; Amassian, A.; et al. Ligand-Stabilized Reduced-Dimensionality Perovskites. *J. Am. Chem. Soc.* **2016**, *138* (8), 2649–2655.

(31) Mitzi, D. B. Synthesis, Crystal Structure, and Optical and Thermal Properties of (C 4 H 9 NH 3) 2 MI 4 (M = Ge, Sn, Pb). *Chem. Mater.* **1996**, *8* (3), 791–800.
(32) Cao, D. H.; Stoumpos, C. C.; Farha, O. K.; Hupp, J. T.; Kanatzidis, M. G. 2D Homologous Perovskites as Light-Absorbing Materials for Solar Cell Applications. *J. Am. Chem. Soc.* **2015**, *137* (24), 7843–7850.
(33) Stoumpos, C. C.; Cao, D. H.; Clark, D. J.; Young, J.; Rondinelli, J. M.; Jang, J. I.; Hupp, J. T.; Kanatzidis, M. G. Ruddlesden–Popper Hybrid Lead Iodide Perovskite 2D Homologous Semiconductors. *Chem. Mater.* **2016**, *28*, 2852–2867.
(34) Passarelli, J. V.; Fairfield, D. J.; Sather, N. A.; Hendricks, M. P.; Sai, H.; Stern, C. L.; Stupp, S. I. Enhanced Out-of-Plane Conductivity and Photovoltaic Performance in n = 1 Layered Perovskites through Organic Cation Design. *J. Am. Chem. Soc.* **2018**, *140* (23), 7313–7323.
(35) Lee, J. K.; Ma, W. L.; Brabec, C. J.; Yuen, J.; Moon, J. S.; Kim, J. Y.; Lee, K.; Bazan, G. C.; Heeger, A. J. Processing Additives for Improved Efficiency from Bulk Heterojunction Solar Cells. *J. Am. Chem. Soc.* **2008**, *130* (11), 3619–3623.
(36) Stoumpos, C. C.; Malliakas, C. D.; Kanatzidis, M. G. Semiconducting Tin and Lead Iodide Perovskites with Organic Cations: Phase Transitions, High Mobilities, and Near-Infrared Photoluminescent Properties. *Inorg. Chem.* **2013**, *52* (15), 9019–9038.
(37) Snaith, H. J.; Hacke, P. Enabling Reliability Assessments of Pre-Commercial Perovskite Photovoltaics with Lessons Learned from Industrial Standards. *Nat. Energy* **2018**, *3* (6), 459–465.
(38) Zuo, L.; Guo, H.; DeQuilettes, D. W.; Jariwala, S.; De Marco, N.; Dong, S.; DeBlock, R.; Ginger, D. S.; Dunn, B.; Wang, M.; et al. Polymer-Modified Halide Perovskite Films for Efficient and Stable Planar Heterojunction Solar Cells. *Sci. Adv.* **2017**, *3* (8), 1–12.
(39) Im, J.-H.; Lee, C.-R.; Lee, J.-W.; Park, S.-W.; Park, N.-G. 6.5% Efficient Perovskite Quantum-Dot-Sensitized Solar Cell. *Nanoscale* **2011**, *3* (10), 4088.
(40) Derjaguin, B. V; Muller, V. M.; Toporov, Y. U. P. Effect of Contact Deformation on the Adhesion of Particles. *J. Colloid Interface Sci.* **1975**, *52* (3), 105–108.
(41) Ahn, N.; Son, D. Y.; Jang, I. H.; Kang, S. M.; Choi, M.; Park, N. G. Highly Reproducible Perovskite Solar Cells with Average Efficiency of 18.3% and Best Efficiency of 19.7% Fabricated via Lewis Base Adduct of Lead(II) Iodide. *J. Am. Chem. Soc.* **2015**, *137* (27), 8696–8699.
(42) Rakita, Y.; Cohen, S. R.; Kedem, N. K.; Hodes, G.; Cahen, D. Mechanical Properties of APbX3 (A=Cs or CH3NH3; X=I or Br) Perovskite Single Crystals. *Arxiv Prepr.* **2015**, *3*, 1–20.
(43) Koczkur, K. M.; Mourdikoudis, S.; Polavarapu, L.; Skrabalak, S. E. Polyvinylpyrrolidone (PVP) in Nanoparticle Synthesis. *Dalt. Trans.* **2015**, *44* (41), 17883–17905.
(44) Yang, J.; Siempelkamp, B. D.; Mosconi, E.; De Angelis, F.; Kelly, T. L. Origin of the Thermal Instability in CH 3 NH 3 PbI 3 Thin Films Deposited on ZnO. *Chem. Mater.* **2015**, *27* (12), 4229–4236.
(45) Nguyen, W. H.; Bailie, C. D.; Unger, E. L.; Mcgehee, M. D. Enhancing the Hole-Conductivity of Spiro-OMeTAD without Oxygen or Lithium Salts by Using Spiro(TFSI) 2 in Perovskite and Dye- Sensitized Solar Cells. *J. Am. Chem. Soc.* **2014**, *136*, 10996–11001.
(46) Jacobsson, T. J.; Correa-Baena, J. P.; Halvani Anaraki, E.; Philippe, B.; Stranks, S. D.; Bouduban, M. E. F.; Tress, W.; Schenk, K.; Teuscher, J.; Moser, J. E.; et al. Unreacted

PbI2 as a Double-Edged Sword for Enhancing the Performance of Perovskite Solar Cells. *J. Am. Chem. Soc.* **2016**, *138* (32), 10331–10343.

(47) Zhang, T.; Guo, N.; Li, G.; Qian, X.; Zhao, Y. A Controllable Fabrication of Grain Boundary PbI2nanoplates Passivated Lead Halide Perovskites for High Performance Solar Cells. *Nano Energy* **2016**, *26*, 50–56.

(48) Zhao, Y.; Nardes, A. M.; Zhu, K. Mesoporous Perovskite Solar Cells: Material Composition, Charge-Carrier Dynamics, and Device Characteristics. *Faraday Discuss.* **2014**, *176*, 301–312.

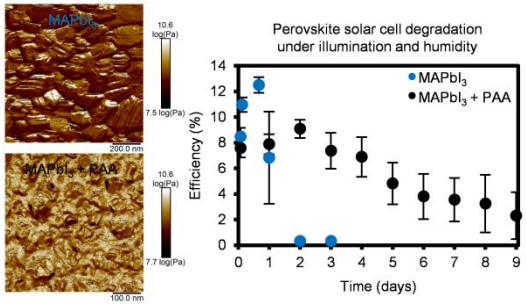

Chemical and morphological origins of the improved stability in various polymer-perovskite hybrid thin films under ambient environmental conditions are investigated.